Structure and dynamics of concentrated dispersions of polystyrene latex spheres in glycerol: Static and dynamic x-ray scattering

D. Lumma, L. B. Lurio, M. A. Borthwick, P. Falus, and S. G. J. Mochrie*
Department of Physics and Center for Materials Science and Engineering, Massachusetts Institute of Technology, Cambridge, Massachusetts 02139-4307
(Received 7 February 2000)

X-ray photon correlation spectroscopy and small-angle x-ray scattering measurements are applied to characterize the dynamics and structure of concentrated suspensions of charge-stabilized polystyrene latex spheres dispersed in glycerol, for volume fractions between 2.7% and 52%. The static structures of the suspensions show essentially hard-sphere behavior. The short-time dynamics shows good agreement with predictions for the wave-vector-dependent collective diffusion coefficient, which are based on a hard-sphere model [C. W. J. Beenakker and P. Mazur, Physica A **126**, 349 (1984)]. However, the intermediate scattering function is found to violate a scaling behavior found previously for a sterically stabilized hard-sphere suspension [P. N. Segre and P. N. Pusey, Phys. Rev. Lett. **77**, 771 (1996)]. Our measurements are parametrized in terms of a viscoelastic model for the intermediate scattering function [W. Hess and R. Klein, Adv. Phys. **32**, 173 (1983)]. Within this framework, two relaxation modes are predicted to contribute to the decay of the dynamic structure factor, with mode amplitudes depending on both wave vector and volume fraction. Our measurements indicate that, for particle volume fractions smaller than about 0.30, the intermediate scattering function is well described in terms of single-exponential decays, whereas a double-mode structure becomes apparent for more concentrated systems.

PACS number(s): 82.70.Dd, 05.40.−a, 83.10.Pp

I. INTRODUCTION

Dispersions of spherical particles with effectively hard-sphere interactions are the simplest complex fluids. Indeed, one may hope to build understanding of more complicated soft matter on the behavior of colloidal dispersions. It is therefore notable that after more than 20 years of research [1–4] the dynamics of colloidal particles with hard-sphere interactions are still not fully understood. The ability to prepare colloidal suspensions, composed of nearly perfectly spherical, highly monodisperse nanoscale particles dispersed in a liquid [5–7], enables experiments on accurate realizations of hard spheres. Moreover, because colloidal particles are much larger than atoms and molecules, a variety of experimental methods can be applied, which permit detailed studies of the structure and dynamics on the length and time scales relevant to individual particles [8–13].

In this article, we present static and dynamic x-ray scattering measurements of the structure and dynamics of concentrated colloidal suspensions of charge-stabilized polystyrene (PS) spheres dispersed in glycerol for volume fractions from a few percent up to the crystallization limit. Our goal is to elucidate how particle diffusion is modified as the motions of the particles become increasingly constrained by the presence of neighbors, as necessarily occurs at large volume fractions. Insofar as their static structure and phase behavior is concerned, these dispersions show essentially hard-sphere interactions. However, their dynamics appear to present significant differences from the dynamical behavior observed experimentally [8,14] for the prototypical hard-sphere system of poly(methyl methacrylate) (PMMA) spheres, sterically stabilized with a grafted layer of poly(hydroxy steric acid) (PHSA), and suspended in decalin/tetralin mixtures [15].

Because of the refractive index difference $n_{PS}-n_{Gl}$ between polystyrene ($n_{PS}\simeq 1.59$) and glycerol ($n_{Gl}\simeq 1.47$), our suspensions are milky in appearance, as a result of strong multiple scattering of light. Consequently, it would be very difficult to carry out light scattering studies of the dynamic mode structure and static correlations in any of the highly concentrated samples considered, even using the two-color technique [8]. Instead, we have applied the emerging technique of x-ray photon correlation spectroscopy (XPCS), which employs the principles of dynamic light scattering, but uses x-ray photons from a high-brilliance synchrotron rather than laser light [16–23]. To characterize the system's static structure, simultaneous small-angle x-ray scattering (SAXS) measurements were performed. Multiple scattering of x rays occurs only for unusually strong scatterers, and was of no concern for the present study.

A. Interactions and phase behavior

PS spheres in glycerol, a polar solvent, constitute a prototypical colloidal system. Their interactions, the so-called Derjaguin-Landau-Verwey-Overbeek (DLVO) interactions, are representative of a large class of colloids, consisting of a screened electrostatic repulsion between charges at the spheres' surfaces, plus a longer-ranged, attractive van der Waals component [5–7]. Frequently, colloidal particles interacting via DLVO interactions are taken to have effectively hard-sphere interactions [10]. This hypothesis has found recent support in elegant experiments demonstrating that

*Present address: Departments of Physics and Applied Physics, Yale University, New Haven, CT 06520.

screened, charged polystyrene colloids behave according to the hard-sphere equation of state [24]. For PS spheres in glycerol, SAXS measurements, described below, demonstrate that the interactions between spheres are indistinguishable from those of hard spheres.

In hard-sphere systems, temperature plays no role for the static properties, and the phase behavior depends only on volume fraction [25]. For volume fractions up to 0.494, the equilibrium phase is a colloidal fluid, while above volume fractions of 0.545 one finds a colloidal crystal [4]. Between volume fractions of 0.494 and 0.545, one expects coexistence of the liquid phase at the freezing density of 0.494 and the solid phase at the melting density of 0.545. Within this range, it has been found experimentally that the liquid phase is metastable for volume fractions up to 0.58; beyond about 0.58, large-scale diffusion ceases, corresponding to the appearance of a colloidal glass phase [9]. The effect of a size distribution, i.e., polydispersity, on the fluid-solid transition of hard spheres has been considered in Refs. [26–28], for example. For polydispersities up to about 0.025, corresponding to the system studied here, there is little effect. For larger polydispersities, however, both the freezing and melting densities increase while the difference in their densities decreases.

B. Dynamical behavior

In a dilute colloidal suspension, the diffusion equation can be expected to provide a good description of the low-frequency dynamics, predicting that density fluctuations relax exponentially in time. Similarly, the normalized intermediate scattering function may be described by a single-exponential decay with a relaxation rate $\Gamma = D_0 Q^2$, where D_0 is the free-particle Stokes-Einstein diffusion coefficient, and Q the scattering wave vector. In denser colloidal systems, the wave-vector dependence of Γ is modified through the effect of interparticle correlations, and the intermediate scattering function may not retain its single-exponential form. For such cases it is sensible to define a time- and wave-vector-dependent diffusion coefficient $D(Q,t)$. All dynamical information of the system is then contained in this quantity, which simplifies to a constant in the dilute limit [14]. For PS spheres in glycerol, our measurements indeed show that density relaxation via a single-exponential decay persists up to volume fractions of about 0.30. At higher volume fractions, we observe a more complex decay characterized, however, by different exponential behavior at short and long times. It is convenient, then, to introduce short-time and long-time diffusion coefficients $D_S(Q) = D(Q,0)$ and $D_L(Q) = D(Q,\infty)$.

In this regard, our results are qualitatively similar to those of Ref. [14]. One simple model giving rise to a double-exponential relaxation supposes that neighboring particles may form a ''cage'' about a given particle. For sufficiently short times, the system would then appear to be in a transient equilibrium state, in which every particle would occupy a potential minimum formed via the interactions with its neighbors. On this time scale, whose upper limit is given by the configurational relaxation time, the fluid would exhibit a certain degree of rigidity. Accordingly, one might expect a fast relaxation mode due to collective diffusive behavior within a transient equilibrium state, as well as a long-time relaxation mode due to the decay of these large-scale configurations.

In a colloidal dispersion, each particle experiences the effects of the fluid flow caused by neighboring particles, in addition to random thermal motions. This hydrodynamic interaction plays an important role in the particle's diffusion, although it does not affect the static structure. The principal obstacle preventing a detailed theoretical understanding of diffusion in hard-sphere colloidal suspensions remains the difficulty of fully treating near-field many-body hydrodynamic interactions, which are especially relevant to the dynamics of particles that may approach each other closely, such as sterically stabilized colloids and charge-stabilized colloids with short screening lengths. Beenakker and Mazur evaluated $D_S(Q)$ for hard-sphere diffusion, taking into account many-body hydrodyamic interactions [29]. Recently, Segre and co-workers carried out simulations of hard-sphere diffusion based on a fluctuating lattice Boltzmann method [8]. For charged suspensions, where the particles are well separated, an effective hydrodynamic pair interaction suffices [30,31].

In Ref. [8], Segre and co-workers presented comprehensive measurements of $D_S(Q)$ for hard-sphere colloidal particles: PMMA spheres of 178 nm radius, sterically stabilized with PHSA in decalin/tetralin. They report excellent agreement between these measurements of the short-time diffusion coefficient and their own simulations, both presented in Ref. [8]. The most striking feature of these and earlier results [32–34] is the strong wave-vector dependence about the wave vector corresponding to the peak of the static structure factor. Specifically, the inverse of the diffusion coefficient displays a peak that mimics the peak in the static structure factor. This informs us that low-free-energy configurations, signaled by a peak in the static structure factor, are also long lived, signaled by the corresponding peak in the inverse of the diffusion coefficient. This link between structure and dynamics is well known [35–39]. In fact, our results for the short-time wave-vector-dependent diffusion coefficient are similar to those of Ref. [8]. They agree quite well with the predictions of Ref. [29], especially for low and intermediate volume fractions. Measurements of $D_S(Q)$ in several other concentrated dispersions are described in Refs. [40–42].

We do not know of any theoretical prediction for the full time dependence of $D(Q,t)$. Tokuyama and Oppenheim [43] have presented calculations of the short-time and long-time self-diffusion coefficients, including hydrodynamic interactions, which can be expected to be comparable to our measurements at wave vectors where the static structure factor is unity. We are, however, unaware of any calculations or simulations of $D_L(Q)$ for concentrated hard spheres. For well-separated, charged colloids, the effective hydrodynamic pair interaction can be sensibly employed to predict $D_L(Q)$ [44]. Long-time diffusion in systems of the latter sort was studied experimentally in Refs. [45,46].

C. Proposed scaling forms

The first detailed experimental study of the wave-vector-dependence of long-time diffusion of hard-sphere colloids was carried out for PMMA particles of 178 nm radius, sta-

bilized with PHSA by Segre and Pusey [14]. They suggested a remarkable scaling property obeyed by $D(Q,t)$, offering the promise that the dynamics of strongly interacting hard spheres could be tremendously simplified. Specifically, they found that the wave-vector-dependent short-time diffusion coefficient $D_S(Q)$ was accurately proportional to the long-time diffusion coefficient $D_L(Q)$ over the entire range of wave vectors studied from $QR \simeq 1$ to $QR \simeq 7$. For wave vectors greater than about $QR \simeq 2.5$, they also observed that the ratio of the time- and wave-vector-dependent diffusion coefficient $D(Q,t)$ to the short-time diffusion coefficient $D_S(Q)$ displays no significant wave-vector dependence. Consequently, the functional form $D(Q,t)/D_S(Q)$, plotted versus time at different wave vectors, will collapse onto a time-dependent master curve. A similar collapse, or ''scaling,'' is observed for the normalized intermediate scattering function itself if the form $Q^{-2}D_S^{-1}(Q)\ln f(Q,t)$ is plotted versus delay time t. Even more remarkably, Segre and Pusey were able to show that the quantity $[D(Q,t)-D_L(Q)]/[D_S(Q)-D_L(Q)]$ is a scaling form that appeared to be invariant under change of both wave vector and volume fraction. If plotted versus delay time for wave vectors larger than $QR \simeq 2.7$ and volume fractions in the range $0.38 \leqslant \phi \leqslant 0.494$, this functional form collapses onto a time-dependent master curve. It should be noted that at a fixed wave vector the ratio $D_S(Q)/D_L(Q)$ varies considerably over this range of volume fractions.

In the present article, however, we will show that the proposed scaling appears to be quite delicate, even in ostensibly hard-sphere suspensions. Specifically, we do not observe proportionality between the wave-vector-dependent short- and long-time diffusion coefficients. Consequently, the intermediate scattering function cannot exhibit the scaling observed by Segre and Pusey. The discrepancies between the earlier measurements on PMMA spheres in decalin/tetralin and our measurements on PS spheres in glycerol indicate that the dynamical behavior in sterically stabilized systems is distinct from that of charge-stabilized systems, even though differences in the static structure are negligible. In this regard, it may be pertinent to recall the observation [15] that the low-shear-rate viscosities of ''hard-sphere dispersions'' appear to fall into two bands. The higher-viscosity band includes the results of several measurements performed on PMMA-PHSA dispersions; the lower-viscosity band includes measurements on PS and silica suspensions in both aqueous and nonaqueous liquids [47].

This article is organized as follows. In Sec. II A, we describe the experimental setup employed for the measurements presented in this article, the synchrotron beamline 8-ID at the Advanced Photon Source in Argonne, IL. Section II B details how time-resolved x-ray scattering data are reduced to intensity time autocorrelation functions. The sample preparation is described in Sec. II C. In Secs. III A and III B, we present the theory for and the measurements of the static x-ray scattering cross section, respectively. A theoretical framework for interpreting measurements of the intensity autocorrelation function of concentrated suspensions is described in Sec. IV A. The dynamic measurements themselves are described in Sec. IV B. In Sec. V, we summarize our results.

II. EXPERIMENTAL METHODS

The technique of XPCS applies the well-known principles of dynamic light scattering to x-ray scattering patterns. In general, a dynamic sample illuminated by partially coherent light gives rise to a time-varying speckle pattern. Time autocorrelation of the speckle pattern then yields the characteristic relaxation times of the sample. Specifically, the intensity-intensity time autocorrelation function $g_2(t)$ is defined by

$$g_2(t) = \frac{\langle I(t)I(0)\rangle_E}{\langle I\rangle_E^2}, \tag{1}$$

where $I(t)$ is the detected photon count rate at time t, and $\langle\cdots\rangle_E$ denotes an ensemble average. This quantity can be related to the intermediate scattering function of the sample $S(Q,t)$ via

$$g_2(t) = 1 + A[f(Q,t)]^2, \tag{2}$$

where $f(Q,t) = S(Q,t)/S(Q)$ is the normalized intermediate scattering function. The quantity $S(Q) = S(Q,0)$ denotes the static structure factor, and A refers to the speckle contrast. For a colloidal suspension,

$$S(Q,t) = \frac{1}{N}\sum_{i=1}^{N}\sum_{j=1}^{N}\langle e^{-i\mathbf{Q}\cdot[\mathbf{r}_i(0)-\mathbf{r}_j(t)]}\rangle_E, \tag{3}$$

where $\mathbf{r}_i(t)$ is the position of particle i at time t.

Performing XPCS measurements requires an experimental setup capable of producing speckled scattering images, that is, a beamline allowing for a nonzero optical contrast A. Moreover, one must devise a data analysis technique that is suitable for reducing sequences of speckled scattering images to correlation functions as defined in Eq. (1).

A. Beamline layout

The measurements described in this article were carried out at beamline 8-ID of the Advanced Photon Source. Details of the setup are presented elsewhere [48]. Briefly, we employed x rays of energy 7.66 keV produced by a 72-pole undulator. The undulator has effective Gaussian source sizes of $\sigma_h = 350\ \mu$m and $\sigma_v = 50\ \mu$m in the horizontal and vertical directions, respectively. Radiation originating in the undulator subsequently passes through an aperture with a diameter of $300\ \mu$m, followed by a set of adjustable slits. These two elements minimize cooling requirements on the downstream optics without reducing the useful brilliance of the source. In addition, they limit the effective horizontal source size as viewed from the sample.

A silicon mirror and a germanium monochromator then select a relative full width at half maximum energy bandwidth of 3×10^{-4}. A set of precision crossed slits, 55 m from the undulator source and 40 cm upstream of the sample, determine the spatial dimensions of the beam illuminating the sample. For the measurements reported here, we employed two different slit sizes, $20\ \mu\text{m}\times 50\ \mu$m and $40\ \mu\text{m}\times 50\ \mu$m in the horizontal $\times$ vertical dimensions. With the smaller slit setting, the partially coherent x-ray beam delivered to the sample at 8-ID contains about 2×10^{10} x rays per second at a synchrotron ring current of

100 mA. Scattered x rays are detected 4.85 m further downstream using a two-dimensional charge-coupled device (CCD) detector.

The quantity measured in XPCS experiments is the normalized intensity autocorrelation function, triangularly averaged over the accumulation time, and coarse-grained over the pixel area. The effects of both averages, as well as the coherence properties of the beamline, are modeled in Ref. [48]. For the parameters appropriate to the present experiment, we expect a contrast of order $A \simeq 0.10$–0.20, depending on the settings determining the effective source size and the illuminated sample area.

B. Data reduction

Dynamical properties of the suspensions were characterized via autocorrelation of sequences of CCD images. Area detectors can expedite the study of slow dynamics in the regime of short data batches, defined as measurements whose total duration does not significantly exceed the coherence time of the sample under study. The latter is the regime in which our XPCS measurements are carried out. The detection scheme by means of a two-dimensional CCD allows data to be acquired from many speckles simultaneously, and offers the possibility of mitigating the difficulty posed by the small photon count rates encountered in XPCS measurements [18,21,22]. Combining this advantage with the benefits of the azimuthal information afforded by a two-dimensional detector, it becomes clear that the use of an area detector in XPCS measurements enables a fundamental improvement in data quality over what would be possible by use of a single detector channel.

Employing a data reduction procedure described in Ref. [48], we were able to probe intensity autocorrelation functions for delay times from 30 ms to more than 100 s. The calculational procedures for reducing sequences of speckled scattering images to correlation functions, as defined in Eq. (1), have been implemented in a code written in the interpreted YORICK language [49]. The code provides a simultaneous evaluation of the correlation function $g_2(\overline{Q}_i,t)$ on a set of detector subregions with mean scattering wave vector $\overline{Q}_i$. For an isotropic sample, such as the colloidal suspension discussed in the present case, the azimuthal degree of freedom in reciprocal space allows one to determine an absolute value for the normalized correlation function from data sets that cover only a fraction of the coherence time of the sample. Similarly, this detection scheme provides a direct measure of the statistical uncertainties in the measured correlation functions. All error bars on the dynamic measurements presented in this article are ultimately based on this experimental determination of statistical uncertainty. The statistical noise performance of different estimators for Eq. (1), as well as the bias occurring in estimating the correlation function mean, are discussed in Ref. [48].

C. Suspensions of polystyrene spheres in glycerol

Polystyrene latex spheres suspended in glycerol, which is a polar solvent, constitute a prototypical system for which the DLVO interactions are representative of a large class of colloids [5]. Glycerol was chosen as the suspending medium to slow down the dynamics, permitting time-resolved measurements of the x-ray speckle pattern using the CCD detector [18,50]. A further benefit of choosing to study PS spheres in glycerol is that the density difference between polystyrene and glycerol is close to 0.2 $\mathrm{g\,cm^{-3}}$, corresponding to an electron number density difference of 6 $\mathrm{electrons\,nm^{-3}}$. This electron number density difference is about four times larger than that between polystyrene and water, making the scattered intensity for a PS-glycerol system 16 times larger than that for a comparable PS-water system. We may also note that, because the refractive index of glycerol is closer to that of PS than to that of water, the van der Waals attraction between particles is expected to be three times smaller for PS spheres in glycerol than for identical spheres in water.

To prepare the samples, an aqueous suspension containing PS latex particles with a nominal radius of 71 nm was purchased from Duke Scientific. The nominal colloidal volume fraction was 0.10. The relative standard deviation in radius was quoted to be 0.025, which was found to be consistent with dynamic light scattering measurements performed at MIT on a very dilute sample. By using colloidal particles with this relatively small polydispersity, we may hope to avoid complications due to a size distribution of finite width. Known weights of the as-received suspension were mixed with known weights of glycerol. The water was then removed by evaporation, under vacuum, leaving the PS spheres suspended in glycerol. Samples were manufactured with sphere volume fractions of $\phi = 0.027$, 0.13, 0.28, 0.34, 0.49, and 0.52, determined on the basis of the nominal volume fraction of the as-received suspension. For the x-ray measurements, the samples were mounted in the evacuated, temperature-controlled sample chamber and cooled to a temperature of $-5\,^{\circ}\mathrm{C}$. We estimated the temperature stability to be better than $\pm 0.03\,^{\circ}\mathrm{C}$, and the absolute precision to be $\pm 0.2\,^{\circ}\mathrm{C}$.

III. STATIC STRUCTURE

This section will present the static characterization of our colloidal system by means of SAXS. We will introduce the topic by summarizing the most relevant theoretical expectations, and will continue with a description of our experimental data. The section will close with a discussion of the static data.

A. X-ray scattering cross section: Theoretical background

The scattering cross section per unit volume $\Sigma(Q)$ is defined in terms of the rate of incident x rays, n_i, and the rate of scattered x rays, n_s, via

$$\frac{n_s}{n_i} = \Sigma W \Delta\Omega, \tag{4}$$

where W denotes the sample thickness along the beam and $\Delta\Omega$ the solid angle over which the rate n_s is detected. We may focus on the case pertinent to the present article, namely, a collection of N nearly identical spherical particles suspended in a fluid. If all of the particles are treated as identical, then the cross section may be expressed as

$$\Sigma = \delta\rho^2 r_0^2 v\, \phi P(Q) S(Q), \tag{5}$$

where $\delta\rho$ is the difference in electron number density between the particles and the fluid. Moreover, r_0 denotes the Thomson radius, v the volume of a colloidal particle, $\phi = Nv/V$ the overall particle volume fraction, $P(Q)$ the particle form factor, and

$$S(Q) = \frac{1}{N}\sum_{i=1}^{N}\sum_{j=1}^{N}\langle e^{-i\mathbf{Q}\cdot(\mathbf{r}_i-\mathbf{r}_j)}\rangle_E = 1 + \frac{4\pi\phi}{v}\int_0^\infty dr r^2[g(r)-1]\frac{\sin Qr}{Qr} \tag{6}$$

the static structure factor. The quantity $g(r)$ refers to the radial pair correlation function.

A closed-form expression for the static structure factor of a system of spheres interacting via hard-sphere interactions, $S_0(Q)$, is available based on Percus-Yevick [1] closure relations:

$$\frac{1}{S_0(Q)} = 1 + \frac{24\phi}{u^3}\left\{ a(\sin u - u\cos u) + b\left[\left(\frac{2}{u^2}-1\right)u\cos u + 2\sin u - \frac{2}{u}\right] + \frac{\phi a}{2}\left[\frac{24}{u^3} + 4\left(1-\frac{6}{u^2}\right)\sin u - \left(1-\frac{12}{u^2}+\frac{24}{u^4}\right)u\cos u\right]\right\}, \tag{7}$$

with $u = 2QR$. The quantity R denotes the hard-sphere radius, $a = (1+2\phi)^2(1-\phi)^{-4}$, and $b = -\frac{3}{2}\phi(\phi+2)^2(1-\phi)^{-4}$. In fact, using a Percus-Yevick closure, it is possible to calculate the cross section for a collection of spheres with radii distributed according to a generalized exponential distribution [51,52]. However, the structure factors of monodisperse spheres and spheres with a relative polydispersity of 0.025 in radius are very similar.

The small-wave-vector limit of the static structure factor of a suspension of monodisperse particles is related to the osmotic compressibility κ_T via

$$S(0) = \phi k_B T \kappa_T. \tag{8}$$

For monodisperse hard spheres in the Percus-Yevick approximation, it follows from Eq. (7) that $S_0(0) = (1-\phi)^4/(1+2\phi)^2$.

B. X-ray scattering cross section: Experiment

Static x-ray scattering measurements are carried out by collecting scattering patterns with a two-dimensional CCD area detector. Figure 1 shows a typical gray-scale image obtained at 8-ID of the scattering from PS particles with a diameter of 66.5 nm, suspended in glycerol. The region of reciprocal space probed covers only a quadrant of the scattering—the direct beam would occur just beyond the top left corner of the image. The smallest wave vector measured ($0.02\ \mathrm{nm}^{-1}$) corresponds to the top left corner of the image and the largest one ($0.2\ \mathrm{nm}^{-1}$) to the bottom right corner. The intensity varies smoothly everywhere and shows circular symmetry about the direct beam position, in accordance with the expected isotropy of the sample. In particular, there are apparently no streaks of scattering that could be associated with parasitic scattering from the slits. Several broad rings of high intensity may be seen in the image, concentric with the direct beam position. The rings at larger wave vectors are the intensity oscillations that are characteristic of uniform, or nearly uniform, spheres. The innermost ring, however, originates in interparticle correlations.

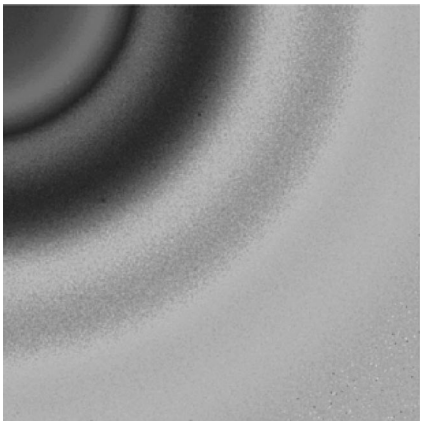

FIG. 1. CCD image showing the scattered intensity from PS latex particles in glycerol at a particle volume fraction of $\phi = 0.49$.

To determine the scattering profiles as accurately as possible, we measured the scattered intensity with the sample in the scattering position and also with the sample removed. To minimize subtraction errors, any localized regions of high parasitic scattering on the CCD were eliminated from consideration. Next, the background scattering patterns—those for which the sample was absent—were appropriately scaled to account for the absorption of the sample and, finally, subtracted from the intensity obtained with the sample in the scattering position. The resulting circularly averaged x-ray scattering cross sections are displayed in Fig. 2 for samples

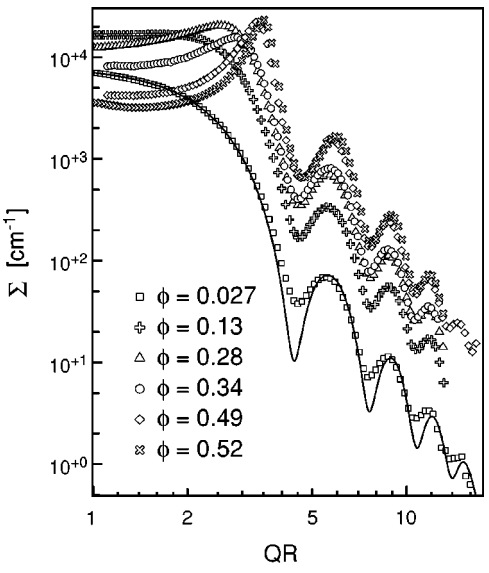

FIG. 2. Circularly averaged scattering cross section per unit volume $\Sigma(QR,\phi)$ for several different volume fractions ϕ of PS latex particles in glycerol. The cross sections are plotted versus QR on a logarithmic scale.

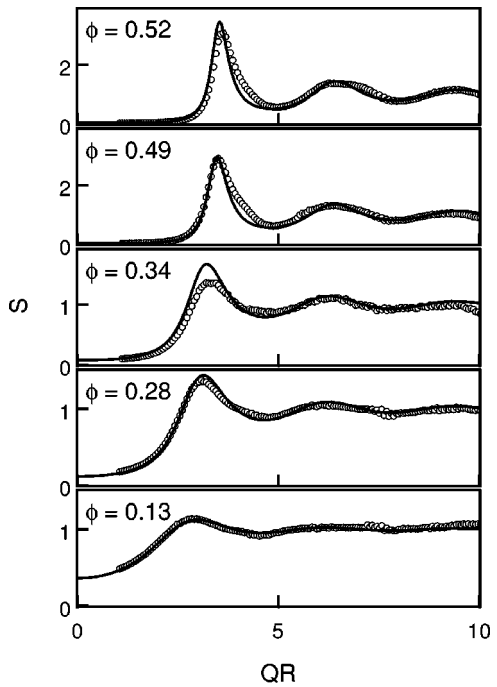

FIG. 3. Interparticle structure factor $S(QR,\phi)$ for PS latex spheres in glycerol for the particle volume fractions indicated. The solid line is the expected static structure factor for particles with a mean radius of 66.5 nm and a relative polydispersity in radius of 0.025, distributed according to a Schultz-Zimm distribution. The structure factors are plotted versus QR on a linear scale.

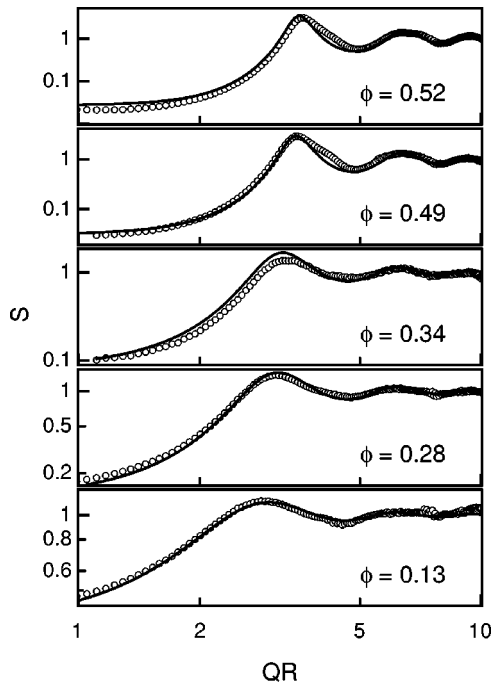

FIG. 4. Interparticle structure factor $S(QR,\phi)$ for PS latex spheres in glycerol for the particle volume fractions indicated. The solid line is the expected static structure factor for particles with a mean radius of 66.5 nm and a relative polydispersity in radius of 0.025, distributed according to a Schultz-Zimm distribution. The structure factors are plotted versus QR on a logarithmic scale.

of different volume fractions and for wave vectors from $QR=1$ to $QR\simeq 15$. The resolution of our setup corresponds to the separation between neighboring data points in Fig. 2.

At large wave vectors, the shape of the scattering curves appears independent of volume fraction and, as noted above, shows the intensity oscillations that are characteristic of uniform spheres. The solid line in Fig. 2 shows the best fit of a model function to the data at a particle volume fraction of $\phi=0.027$. The model describes the scattering of hard spheres with a volume fraction of 0.027 and a relative polydispersity in radius of 0.025. The sole fitting parameter was the mean particle radius, resulting in a best-fit value of 66.5 nm, in fair agreement with the manufacturer's value. The model provides a good description of the data for wave vectors below about 0.06 nm^{-1}. However, it evidently fails to properly describe the behavior at the minima of the cross section. We ascribe the discrepancy to small departures of the colloidal particles from spherical symmetry. Similar behavior was observed in Ref. [53].

At smaller wave vectors, a pronounced peak develops as the volume fraction increases, corresponding to increasing interparticle correlations. This behavior is illustrated in Fig. 3. The figure shows the static structure factor, obtained by dividing the measured scattering for different volume fractions by the particle form factor. The latter was determined from the data at $\phi=0.027$, after applying a small structure factor correction. To make clear the behavior at small wave vectors, where the structure factor is small, Fig. 4 shows these data on a logarithmic scale. They are analogous to the liquid structure factor of an atomic fluid. The principal peak of the structure factor approaches $QR\simeq 3.5$ at large volume fractions, consistent with what may be expected for hard spheres. By contrast, colloidal particles with significant long-ranged Coulomb repulsions can be expected to exhibit a larger mean separation, so that the first peak of the structure factor would occur at smaller wave vectors, with a greater degree of ordering at lower volume fractions. The solid lines in Figs. 3 and 4 correspond to the model structure factor for particles with a mean radius of 66.5 nm and a polydispersity in radius of 0.025, distributed according to a Schultz-Zimm distribution [52]. This model was fitted to the measured structure factor, varying only the volume fraction for each data set.

Evidently, the hard-sphere model provides a good description of the experimental structure factors at all volume fractions, in particular reproducing the position of the principal peak accurately. Gratifyingly, the best-fit values for the volume fractions of the different samples are indistinguishable from the nominal volume fractions. It is, in addition, especially notable that the behavior of the measured structure factor at small wave vectors is reproduced well by the model. This informs us that the osmotic compressibility of PS latex spheres in glycerol is well described by the hard-sphere equation of state. In this regard, two remarks are pertinent. First, if there were significant attractive interactions between particles, we would expect increased scattering at small wave vectors [54], especially for the samples of lower volume fraction. Second, according to Ref. [52], a relative polydispersity of 0.025 can be expected to increase the scattering of a hard-sphere suspension at small wave vectors by less than 2%, compared to the scattering from monodisperse spheres.

We view the agreement between the model and measured structure factors at small wave vectors, as well as the agreement between the measured and predicted positions of the

principal peak in the structure factor, as convincing evidence that PS spheres in glycerol behave as hard spheres. It is apparent, however, that the structure factors measured for particle volume fractions of 0.49 and 0.52 differ somewhat from the model. We believe that this may reflect shortcomings of the analytic model for the structure factor of hard spheres at high volume fractions. Simulations of hard spheres at high volume fractions do reveal discrepancies with the Percus-Yevick form [55,56].

Apart from the discrepancy between the data and the model for $\phi=0.34$ at the first peak of the structure factor, which we do not understand, the most noticeable other difference is that the measurements exhibit a broader second peak than the model. The broader peak may plausibly be interpreted as two broad, closely spaced peaks, occuring at $QR\simeq 6.0$ and $QR\simeq 6.7$. The ''fourth'' peak occurs at $QR\simeq 9.2$, which is at a somewhat smaller value of QR than predicted by the model. The observed ratios of these peak positions to the position of the principal peak, which is located at $QR\simeq 3.5$, are 1.7, 1.9, and 2.7, respectively. Similar ratios are observed for the structure factor of amorphous elemental metallic glasses, prepared by vacuum evaporation onto cooled surfaces [57,58], although it should be emphasized that the metallic glass peaks are narrower and more intense than those found here. In the case of metallic glasses, it has been suggested that these peak position ratios may indicate locally icosahedral structure [59]. Alternatively, random close packing yields similar peak position ratios [57].

IV. DYNAMICS

In the following, the dynamical characterization of our system will be discussed. After a theoretical introduction to the expected phenomena, our experimental findings will be presented. Specifically, the data will be discussed in light of Refs. [8,14], where the dynamical properties of a prototypical hard-sphere system were found to exhibit the specific scaling behavior already described in the introduction. According to Segre and co-workers [8,14], the ratio of the time- and wave-vector-dependent diffusion coefficient to the short-time diffusion coefficient, $D(Q,t)/D_S(Q)$, is independent of wave vector, for wave vectors larger than about $QR\simeq 2.5$. In addition, their data suggest that the functional form $[D(Q,t)-D_L(Q)]/[D_S(Q)-D_L(Q)]$ not only collapses over a similar wave-vector range, but also falls onto the same master curve for a finite range of volume fractions. These findings require that the ratio between short-time and long-time diffusion coefficient, $D_S(Q)/D_L(Q)$, be constant over at least the same wave-vector range. This prerequisite for the proposed scaling behavior could not be confirmed with our measurements.

A. Intensity autocorrelations: Theory

This section aims to present the theoretical framework within which the results of our dynamical measurements will be discussed. At high particle volume fractions, the intermediate scattering functions we observe exhibit single-exponential behavior both at short and at long delay times. The functions are thus naturally characterized by means of least-squares fits to a weighted double-exponential decay, with wave-vector-dependent relaxation rates Γ_F and Γ_L as well as wave-vector-dependent mode amplitudes a_F and a_L. A theoretical treatment applicable to the system considered here is provided by Hess and Klein in Ref. [60]. We show below how in the context of this theory the parameters extracted from a double-exponential decay can be related to more physically defined hydrodynamic properties of the fluid such as the friction coefficient and the rigidity.

Some insight may be obtained by calculating the Laplace transform of the intermediate scattering function, $\tilde{f}(Q,z)$. Supposing that $\tilde{f}(Q,z)$ exhibits simple poles at values of z given by $z=-\Gamma_i$, it follows that the intermediate scattering function in the time domain is given by

$$f(Q,t)=\sum_i a_i e^{-\Gamma_i t}. \tag{9}$$

The mode amplitudes a_i can be derived from the residues of the poles at $z=-\Gamma_i$, via $a_i=\Gamma_i^{-1}\,\mathrm{Res}_{z=-\Gamma_i}\tilde{f}(Q,z)$.

In particular, for concentrated colloidal suspensions, Hess and Klein have shown that the Laplace transform of the intermediate scattering function is of the form

$$\tilde{f}(Q,z)=\frac{1}{z+\dfrac{Q^2k_BT/mS(Q)}{z+\tilde{\zeta}(Q,z)/m}}, \tag{10}$$

where $\tilde{\zeta}(Q,z)$ is a wave-vector- and Laplace-frequency-dependent friction coefficient [60]. The difference between a simple liquid and the colloidal suspension considered in the present case enters into Eq. (10) through the quantity $\tilde{\zeta}(Q,z)$. Colloidal suspensions differ from simple fluids in that neither the momentum nor the energy of the colloidal particles is conserved, because of the coupling to the suspending fluid. As a result, the friction coefficient in Eq. (10) approaches a constant value at small wave vectors, and for the diffusional processes of interest we may neglect z compared to $\tilde{\zeta}(Q,z)$ in the second denominator of Eq. (10). In a simple fluid, by contrast, the friction coefficient varies as Q^2 for small wave vectors, and the z dependence in the second denominator cannot be neglected.

The equilibrium position of each particle in a colloidal fluid is not fixed, so that application of a steady force causes viscous flow. However, for a given particle in a concentrated suspension, one may envisage a transient ''cage'' of neighbors, limiting, as it were, the particle's motional degree of freedom, and thus imposing partial spatial confinement. Dynamically, such a cage structure would be characterized by a length-scale-dependent configurational relaxation time. Over time scales shorter than such a typical configurational relaxation time, an equilibrium position of these partially confined particles is established temporarily. If a force is rapidly applied in this situation, the suspension behaves transiently like an elastic solid, exhibiting an instantaneous rigidity. To describe approximately the response to an applied force, viscoelastic theory interpolates in a simple fashion between fluid-like, viscous flow behavior at low frequencies and solidlike, elastic behavior at high frequencies. Specifically, the friction coefficient is taken to be of the form

$$\tilde{\zeta}(Q,z)=\tilde{\zeta}(Q,\infty)+\Delta\tilde{\zeta}(Q,z). \tag{11}$$

Here we use

$$\Delta\tilde{\zeta}(Q,z)=\frac{R_\infty(Q)-Q^2k_BT/S(Q)}{z+\Gamma_3} \tag{12}$$

and

$$\Gamma_3=\frac{R_\infty(Q)-Q^2k_BT/S(Q)}{\tilde{\zeta}(Q,0)-\tilde{\zeta}(Q,\infty)}. \tag{13}$$

Equation (10) may then be written

$$\tilde{f}(Q,z)=\frac{1}{z+\dfrac{\Gamma_S}{1+\dfrac{\Gamma_2}{z+\Gamma_3}}}, \tag{14}$$

with $\Gamma_S=Q^2k_BT/S(Q)\tilde{\zeta}(Q,\infty)$ and $\Gamma_2=[R_\infty(Q)-Q^2k_BT/S(Q)]/\tilde{\zeta}(Q,\infty)$, where $R_\infty(Q)$ is the high-frequency rigidity. Physically, the variable Γ_3 denotes the strain relaxation rate, while Γ_2 quantifies the extent of coupling between stress and compositional fluctuations. Conventionally, one introduces $D_0=Q^2k_BT/6\pi\eta R$, which is the diffusion coefficient of identical particles in a dilute suspension, and $H(Q)$, which is given by $\tilde{\zeta}(Q,\infty)=6\pi\eta R/H(Q)$, and which accounts for hydrodynamic interactions between the particles. In their absence, $H(Q)$ would take the value unity. Combining these expressions, one obtains $\Gamma_S=H(Q)D_0Q^2/S(Q)$.

According to Eq. (9), the normalized intermediate scattering function corresponding to Eq. (14) is a weighted sum of two exponential decays,

$$f(Q,t)=a_Fe^{-\Gamma_Ft}+a_Le^{-\Gamma_Lt}, \tag{15}$$

with

$$\Gamma_F=\frac{1}{2}(\Gamma_S+\Gamma_2+\Gamma_3)+\frac{1}{2}\sqrt{(\Gamma_S+\Gamma_2+\Gamma_3)^2-4\Gamma_S\Gamma_3},$$

$$\Gamma_L=\frac{1}{2}(\Gamma_S+\Gamma_2+\Gamma_3)-\frac{1}{2}\sqrt{(\Gamma_S+\Gamma_2+\Gamma_3)^2-4\Gamma_S\Gamma_3},$$

$$a_F=\frac{\Gamma_F-(\Gamma_2+\Gamma_3)}{\Gamma_F-\Gamma_L},$$

$$a_L=\frac{(\Gamma_2+\Gamma_3)-\Gamma_L}{\Gamma_F-\Gamma_L}. \tag{16}$$

In writing this, we describe the overall decay of the dynamic structure factor as due to two contributions: a fast decay with relaxation rate Γ_F and mode amplitude a_F, as well as a long-time decay with relaxation rate Γ_L and mode amplitude a_L. As expected, we find that the mode amplitudes sum to unity. In addition, it follows that $\Gamma_S=a_F\Gamma_F+a_L\Gamma_L$, $\Gamma_2=a_Fa_L(\Gamma_F-\Gamma_L)^2/\Gamma_S$, and $\Gamma_3=\Gamma_F\Gamma_L/\Gamma_S$. It is also instructive to note that, for short times,

$$\ln f(Q,t)\simeq\Gamma_S\left(-t+\frac{1}{2}\Gamma_2t^2+\cdots\right). \tag{17}$$

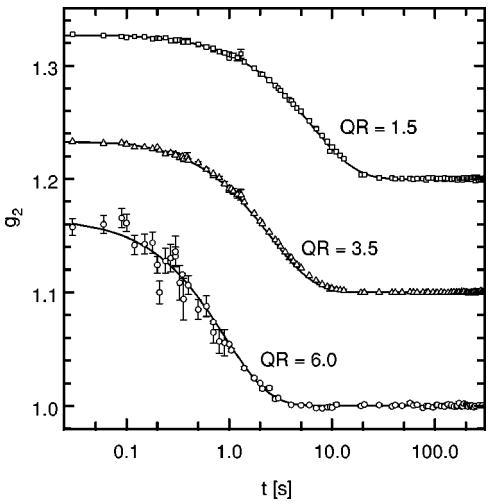

FIG. 5. Intensity autocorrelation functions $g_2(QR,t)$ for PS spheres in glycerol with a volume fraction of $\phi=0.28$, at a temperature of -5 °C, and for wave vectors given by $QR=1.5$, 3.5, and 6.0. Lines are the results of least-squares fits to a model for the intermediate scattering function consisting of a single-exponential decay.

From Eq. (17), it is apparent that Γ_S is the initial, short-time decay rate, so that one may introduce a corresponding short-time, wave-vector-dependent, collective diffusion coefficient $D_S=\Gamma_S/Q^2$. Moreover, Γ_2/Γ_S is the normalized second cumulant of the decay rate distribution [61]. This indicates that Γ_2 is a measure of the width in the decay rate distribution.

Equation (16) has a number of interesting limits. First, if $\Gamma_2=0$, it follows that $\Gamma_L=\Gamma_S$, $\Gamma_F=\Gamma_3$, $a_L=1$, and $a_F=0$, i.e., one observes a single-exponential decay. This result informs us that Γ_S is the relaxation rate of compositional fluctuations in the absence of coupling to stress. Second, for $\Gamma_S+\Gamma_2+\Gamma_3\gg\Gamma_S\Gamma_3$, one finds that $\Gamma_F\simeq\Gamma_S+\Gamma_2+\Gamma_3$, $\Gamma_L\simeq\Gamma_S\Gamma_3/(\Gamma_S+\Gamma_2+\Gamma_3)$, $a_F\simeq\Gamma_S/(\Gamma_S+\Gamma_2+\Gamma_3)$, and $a_L\simeq(\Gamma_2+\Gamma_3)/(\Gamma_S+\Gamma_2+\Gamma_3)$. Third, as noted in Ref. [46], the limit of $\Gamma_3=0$ corresponds to an entirely elastic response, i.e., a crystal, a glass, or a gel. In this case, it follows that $\Gamma_F=\Gamma_S+\Gamma_2$, $\Gamma_L=0$, $a_F=\Gamma_S/(\Gamma_S+\Gamma_2)$, and $a_L=\Gamma_2/(\Gamma_S+\Gamma_2)$.

B. Intensity autocorrelations: Results

Representative intensity autocorrelations for delay times from 30 ms to 300 s, obtained for the samples with $\phi=0.28$ and $\phi=0.52$, are shown at $QR=1.0$, 3.5, and 6.0 in Figs. 5 and 6, respectively. It is clear that the solid lines in Fig. 5, corresponding to single-exponential decays, describe the data at $\phi=0.28$ very well. More generally, for the samples with volume fractions of $\phi=0.027$, 0.13, and 0.28, a single-exponential decay provides a good description of the intensity autocorrelations versus delay time, and hence of the intermediate scattering function, at all wave vectors studied.

By contrast, at $\phi=0.52$, a single-exponential form for the intermediate scattering function does not provide a good description of the intensity autocorrelations, as can be seen in Fig. 6. Nevertheless, we observe that, at both short and long times, $\ln f$ varies linearly with delay time t, in agreement with Eq. (15). Accordingly, following Segre and Pusey, we

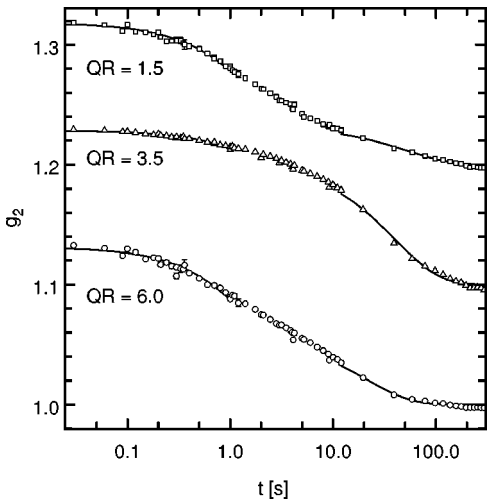

FIG. 6. Intensity autocorrelation functions $g_2(QR,t)$ for PS spheres in glycerol with a volume fraction of $\phi=0.52$, at a temperature of -5 °C, and for wave vectors given by $QR=1.5$, 3.5, and 6.0. Lines are the results of linear least-squares fits within the time ranges at short and long times for which the logarithm of the intermediate scattering function is accurately linear.

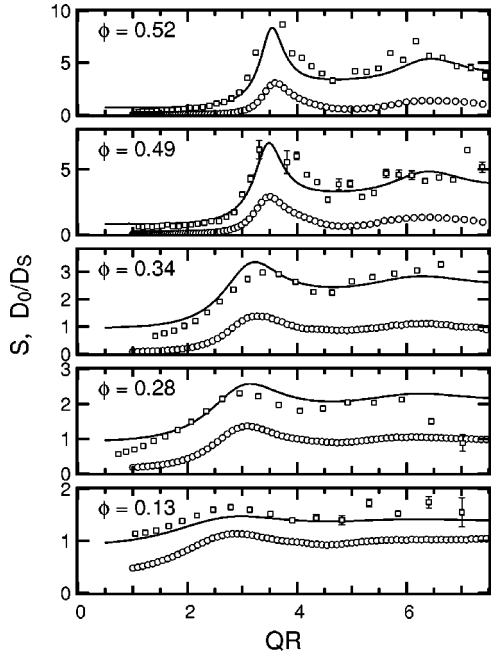

FIG. 7. The open squares display the fitted short-time inverse diffusion coefficient after normalization by the Einstein-Stokes diffusion coefficient D_0/D_S, plotted versus QR for several volume fractions ϕ of PS spheres in glycerol. The solid lines represent the model discussed in the text. The open circles show the static structure factor $S(QR,\phi)$.

may introduce corresponding short-time and long-time diffusion coefficients D_S and D_L, respectively. We determined D_S and D_L by linear least-squares fits over time ranges at short and long times, respectively, within which $(\ln f)$ versus delay time t does not deviate significantly from a straight line. In Fig. 6, the solid lines illustrate the corresponding model autocorrelation functions over the time ranges in question, where they clearly describe the data well. The autocorrelations for the samples with volume fractions of $\phi=0.34$, 0.49, and 0.52 are not well described by a single-exponential form for $f(Q,t)$.

For each of the different samples, the open squares in Fig. 7 display as a function of wave vector our measurements of D_0/D_S, which were obtained from the slope of $\ln f$ at small times. The most striking feature of these and earlier results [33,34,40,41] is that the inverse of the diffusion coefficient displays a peak that mimics the peak in the static structure factor, itself illustrated as the open circles in Fig. 7. This informs us that low-free-energy configurations, signaled by a peak in the static structure factor, are also long-lived, signaled by the corresponding peak in the inverse of the diffusion coefficient. In the absence of hydrodynamic interactions, the wave-vector dependence of the inverse diffusion coefficient would result entirely from the static structure factor [60]. Since it is clear from Fig. 7 that D_0/D_S and $S(Q)$ are not identical, significant hydrodynamic interactions are indicated. Moreover, since $D_0/D_S>S(Q)$, we may infer that hydrodynamic interactions inhibit diffusion at all wave vectors.

Analytic calculations of the wave-vector dependence of D_0/D_S for hard spheres, taking into account many-body hydrodynamic interactions, have been carried out by Beenakker and Mazur [29]. Their predictions, shown as the solid lines, are compared to the present measurements in Fig. 7, showing quantitative agreement.

At long times, only the slow component of Eq. (15) survives, so that the intermediate scattering function decays exponentially at long times as well as at short times. As noted above, one of the principal results of Ref. [14] is that D_S/D_L is independent of wave vector. For example, for $\phi=0.465$, a ratio of $D_S/D_L=4.3$ is reported. The scaling behavior found by Segre and Pusey requires the proportionality of D_S and D_L. Figure 8 shows the ratio of long-time to short-time diffusion coefficients, D_S/D_L, for samples with particle volume fractions of $\phi=0.28$, 0.34, 0.49, and 0.52, plotted versus QR. For all samples with particle volume fractions larger than 0.28, there is a significant wave-vector dependence.

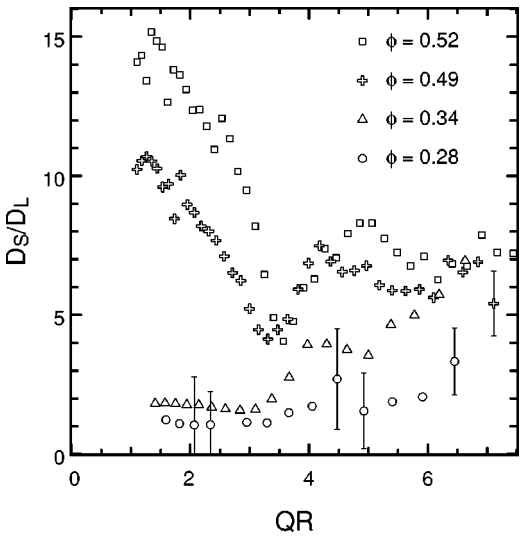

FIG. 8. Ratio of short-time to long-time diffusion coefficients, D_S/D_L, plotted versus QR for several volume fractions ϕ of PS spheres suspended in glycerol.

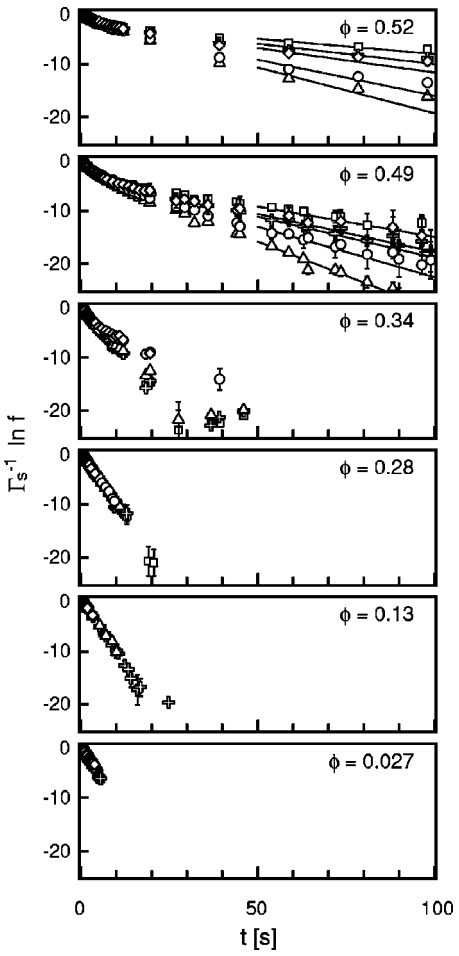

FIG. 9. Logarithm of the intermediate scattering function after normalization by the short-time relaxation rate $\Gamma_S^{-1} \ln f$ for PS spheres in glycerol at the indicated volume fractions ϕ plotted versus delay time. The solid lines represent single-exponential fits to the long-time behavior.

Therefore, our results do not scale in the fashion discovered for sterically stabilized PMMA spheres in decalin/tetralin.

To further examine the extent to which the described scaling behavior is violated for PS spheres in glycerol, we plot $\Gamma_S^{-1} \ln f$ versus delay time and volume fraction in Fig. 9. For $\phi = 0.027$ and 0.13, the data evidently collapse to a single straight line with a slope of -1, as expected for the single-exponential form of the intermediate scattering function at these volume fractions. For the data obtained at $\phi = 0.28$, there appears to be a slight deviation from linear behavior with a slope of -1 at times beyond 5 s. For the samples with volume fractions of $\phi = 0.34$, 0.49, and 0.52, there is a clear deviation from a slope of -1. With increasing volume fraction, this deviation actually occurs at progressively earlier scaled times $D_S Q^2 t$. (Data not shown.) At later times, at each value of QR, there is a crossover to a new linear behavior. The long-time slopes differ from one value of QR to the next, corresponding to different values of D_L/D_S at different values of QR. It is apparent that the data do not reduce to a single curve, so that the proposed scaling behavior is violated.

For completeness, we collect in Fig. 10 the results for a_F/a_L, Γ_F/Γ_L, Γ_2, and Γ_3, deduced from least-squares fits to the measurements on our three most concentrated

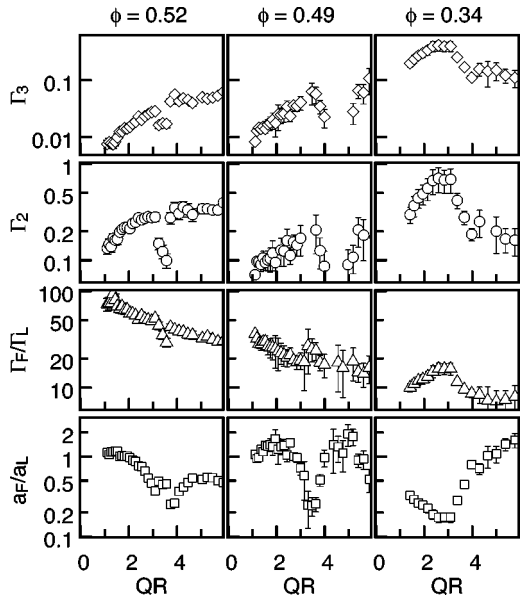

FIG. 10. Ratio of decay rates and mode amplitudes for the double-exponential model discussed in the text, Γ_F/Γ_L and a_F/a_L. Also shown are the relaxation rates Γ_2 and Γ_3. All quantities are plotted for the indicated volume fractions ϕ as a function of QR.

samples. Specifically, we show data for volume fractions of 0.34, 0.49, and 0.52, plotted versus QR. Let us first consider the ratio between the respective amplitudes of the two modes contributing to the decay in Eq. (15). The bottom row of panels in Fig. 10 shows this ratio a_F/a_L. Across all three volume fractions, we find a distinct drop at a value of QR close to that of the principal peak in the static structure factor. Accordingly, the locus of the minimum in a_F/a_L apparently shifts toward slightly smaller values of QR for smaller volume fractions. The fact that we observe a minimum in a_F/a_L at those wave vectors signifies the dominance of the long-time decay for the long-lived, low-free-energy configurations of the sample. In terms of the intuitive physical picture introduced earlier, one might reason that the slow configuration relaxation of a transient ''cage'' structure dominates over faster relaxations due to viscous, localized flow of particles partially confined by their neighbors.

The impact of such caging effects on the relaxation spectrum of a sample would be expected to decrease for smaller particle volume fractions. For in less concentrated systems, the partial confinement of single particles imposed by their neighbors should be less significant, and viscous flow processes should gain more importance for the relaxation of equilibrium fluctuations. In fact, in the extreme limit of a dilute suspension, caging effects have no significance whatsoever. We may qualitatively follow this behavior by considering the ratio Γ_F/Γ_L between the two decay rates in Eq. (15), as shown in Fig. 10. With decreasing volume fraction, the two decay rates become more commmensurate. This might be interpreted to imply that the distinction between a long-time decay corresponding to the relaxation of fluctuations in a transient cage structure on the one hand, and a fast decay corresponding to processes of partially confined diffusion on the other hand, becomes less clearly defined. As was discussed earlier, for particle volume fractions smaller than about 0.30, we observe a single-exponentional decay in the

intermediate scattering function, and the above distinction becomes meaningless. Interestingly, the data for Γ_F/Γ_L exhibit a smooth decrease with QR for particle volume fractions of 0.52 and 0.49. At a volume fraction of 0.34, by contrast, the ratio Γ_F/Γ_L appears to reflect the local extremum in the static structure factor.

In the discussion of Eq. (16), it was pointed out that the limit of $\Gamma_3=0$ describes the regime of an entirely elastic response. Considering the data on Γ_3 presented in Fig. 10, we find that the measured values for Γ_3 are largest at the lowest volume fraction considered, $\phi=0.34$, for all wave vectors probed. We note that the limit $\Gamma_3\rightarrow 0$ is most closely resembled by the data from systems with larger particle volume fractions. This would agree with the expectation that a solid-like, elastic response is most likely to be observed in dense colloidal suspensions, where partial, transient ordering can take place. Finally, in considering the behavior of the decay rate Γ_2 shown in Fig. 10, we again observe a reflection of the broad first-order structure factor peak for a volume fraction of $\phi=0.34$, in contrast to the measurements for the other volume fractions. Overall, it seems as if the extent to which the decay rates are affected by the wave-vector dependence of the liquid structure factor is least significant for the most concentrated sample, at a volume fraction of $\phi=0.52$.

V. CONCLUSION

In conclusion, we have presented a detailed dynamic and static x-ray scattering study of diffusion and structure in a concentrated suspension of hard spheres, PS latex spheres in glycerol. We do not find a previously observed proportionality between short- and long-time diffusion constants, nor scaling behavior. The discrepancies between the results of Ref. [14] and our measurements may be an indication that the dynamical behavior in sterically stabilized systems is distinct from that of charge-stabilized systems, even though differences in the static structure are negligible. In this regard, it may be pertinent to recall the observation [15] that the low-shear-rate viscosities of ''hard-sphere dispersions'' appear to fall into two bands. The higher-viscosity band includes the results of several measurements performed on PMMA-PHSA dispersions; the lower-viscosity band includes measurements on PS and silica suspensions in both aqueous and nonaqueous liquids.

ACKNOWLEDGMENTS

Beamline 8-ID was developed with support from the NSF Instrumentation for Materials Research Program (Grant No. DMR-9312543), from the DOE Facilities Initiative Program (Grant No. DE-FG02-96ER45593), and from NSERC. Work at MIT was also supported by the NSF MRSEC Program (Grant No. DMR-9808941). D.L. acknowledges the JSEP for support. The Advanced Photon Source is supported by the U.S. DOE under Contract No. W-31-109-Eng-38. We thank Bruce Ackerson, Aleksey Lomakin, Amit Malik, Jean-Francois Pelletier, Lynne Regan, Brian Stephenson, and Mark Sutton for their contributions, and Harold Gibson for his expert technical assistance. We greatly benefitted from Gerald Swislow's uncompromising support of our data acquisition software. We are especially indebted to Alec Sandy for his collaboration in the design, implementation, and development of 8-ID.

[1] R. J. Baxter, Aust. J. Phys. **21**, 563 (1968).
[2] B. J. Alder and T. E. Wainwright, J. Chem. Phys. **27**, 1208 (1957).
[3] D. Chandler, J. D. Weeks, and H. C. Andersen, Science **220**, 787 (1983).
[4] W. G. Hoover and F. R. Ree, J. Chem. Phys. **49**, 3609 (1968).
[5] R. J. Hunter, *Foundations of Colloid Science* (Oxford University Press, Oxford, 1989).
[6] P. N. Pusey, *Liquids, Freezing and the Glass Transition* (North-Holland, Amsterdam, 1991), pp. 763–942.
[7] W. C. K. Poon and P. N. Pusey, in *Observation, Prediction, and Simulation of Phase Transitions in Complex Fluids*, edited by M. Baus, L. F. Rull, and J.-P. Ryckaert (Kluwer Academic Publishers, Dordrecht, 1995), pp. 3–51.
[8] P. N. Segre, O. P. Behrend, and P. N. Pusey, Phys. Rev. E **52**, 5070 (1995).
[9] W. van Megan and P. N. Pusey, Phys. Rev. A **43**, 5429 (1991).
[10] A. J. C. Ladd, H. Gang, J. X. Zhu, and D. A. Weitz, Phys. Rev. Lett. **74**, 318 (1995).
[11] C. A. Murray and D. G. Grier, Annu. Rev. Phys. Chem. **47**, 421 (1996).
[12] A. van Blaaderen and P. Wiltzius, Science **270**, 1177 (1996).
[13] R. Verma, J. C. Crocker, T. C. Lubensky, and A. G. Yodh, Phys. Rev. Lett. **81**, 4004 (1998).
[14] P. N. Segre and P. N. Pusey, Phys. Rev. Lett. **77**, 771 (1996).
[15] S.-E. Phan, W. B. Russel, Z. Cheng, J. Zhu, P. M. Chaikin, J. H. Dunsmuir, and R. H. Ottewill, Phys. Rev. E **54**, 6633 (1996).
[16] M. Sutton, S. G. J. Mochrie, T. Greytak, S. E. Nagler, L. E. Berman, G. A. Held, and G. B. Stephenson, Nature (London) **352**, 608 (1991).
[17] S. Brauer, G. B. Stephenson, M. Sutton, R. Brüning, E. Dufresne, S. G. J. Mochrie, G. Grübel, J. Als-Nielsen, and D. L. Abernathy, Phys. Rev. Lett. **74**, 2010 (1995).
[18] S. B. Dierker, R. Pindak, R. M. Fleming, I. K. Robinson, and L. E. Berman, Phys. Rev. Lett. **75**, 449 (1995).
[19] B. Chu, J. C. Ying, F. J. Yeh, A. Patkowski, W. Steffen, and E. W. Fisher, Langmuir **11**, 1419 (1995).
[20] T. Thurn-Albrecht, W. Steffen, A. Patkowski, G. Meier, E. W. Fisher, G. Grübel, and D. L. Abernathy, Phys. Rev. Lett. **77**, 5437 (1996).
[21] S. G. J. Mochrie, A. M. Mayes, A. R. Sandy, M. Sutton, S. Brauer, G. B. Stephenson, D. L. Abernathy, and G. Grübel, Phys. Rev. Lett. **78**, 1275 (1997).
[22] O. K. C. Tsui and S. G. J. Mochrie, Phys. Rev. E **57**, 2030 (1998).
[23] A. C. Price, L. B. Sorensen, S. D. Kevan, J. Toner, A. Poniewierski, and R. Holyst, Phys. Rev. Lett. **82**, 755 (1999).
[24] M. A. Rutgers, J. H. Dunsmuir, Z.-X. Xue, W. B. Russel, and P. M. Chaikin, Phys. Rev. B **53**, 5043 (1996).

[25] M. Adams, Z. Dogic, S. L. Keller, and S. Fraden, Nature (London) **393**, 349 (1998).
[26] S.-E. Phan, W. B. Russel, J. Zhu, and P. M. Chaikin, J. Chem. Phys. **108**, 9789 (1998).
[27] D. A. Kofke and P. G. Bolhuis, Phys. Rev. E **59**, 618 (1999).
[28] P. Bartlett and P. B. Warren, Phys. Rev. Lett. **82**, 1979 (1999).
[29] C. W. J. Beenakker and P. Mazur, Physica A **126**, 349 (1984).
[30] U. Ganz and R. Klein, Physica A **171**, 26 (1991).
[31] G. Nägele, O. Kellerbauer, R. Krause, and R. Klein, Phys. Rev. E **47**, 2562 (1993).
[32] D. W. Schaefer and B. J. Berne, Phys. Rev. Lett. **32**, 1110 (1974).
[33] J. C. Brown, P. N. Pusey, J. W. Goodwin, and R. H. Ottewill, J. Phys. A **8**, 664 (1975).
[34] W. van Megan, R. H. Ottewill, S. M. Owens, and P. N. Pusey, J. Chem. Phys. **82**, 508 (1985).
[35] P. G. de Gennes, Physica (Amsterdam) **25**, 825 (1956).
[36] A. R. Altenberger and J. M. Deutch, J. Chem. Phys. **59**, 894 (1973).
[37] B. J. Ackerson, J. Chem. Phys. **64**, 242 (1976).
[38] A. R. Altenberger, J. Chem. Phys. **70**, 1994 (1979).
[39] P. N. Pusey and R. J. A. Tough, J. Phys. A **15**, 1291 (1982).
[40] A. P. Philipse and A. Vrij, J. Chem. Phys. **88**, 6459 (1988).
[41] J. K. Phalakornkul, A. P. Gast, R. Pecora, G. Nägele, A. Ferrante, B. Mandl-Steininger, and R. Klein, Phys. Rev. E **54**, 661 (1996).
[42] W. Härtl, C. Beck, and R. Hempelmann, J. Chem. Phys. **110**, 7070 (1999).
[43] M. Tokuyama and I. Oppenheim, Phys. Rev. E **50**, R16 (1994).
[44] G. Nägele and P. Baur, Europhys. Lett. **38**, 557 (1997).
[45] F. Grüner and W. Lehmann, J. Phys. A **12**, L303 (1979).
[46] F. Grüner and W. Lehmann, J. Phys. A **15**, 2847 (1982).
[47] T. Shitaka and D. S. Pearson, J. Rheol. **38**, 601 (1994), for example.
[48] D. Lumma, L. B. Lurio, S. G. J. Mochrie, and M. Sutton, Rev. Sci. Instrum. **71**, 3274 (2000).
[49] D. H. Munro, Comput. Phys. **9**, 609 (1995).
[50] A. P. Y. Wong and P. Wiltzius, Rev. Sci. Instrum. **64**, 2547 (1993).
[51] A. Vrij, J. Chem. Phys. **71**, 3267 (1979).
[52] W. L. Griffith, R. Triolo, and A. L. Compere, Phys. Rev. A **35**, 2200 (1987).
[53] B. Chu, Y. Li, P. J. Harney, and F. Yeh, Rev. Sci. Instrum. **64**, 1510 (1994).
[54] X. Ye, T. Narayanan, P. Tong, and J. S. Huang, Phys. Rev. Lett. **76**, 4640 (1996).
[55] W. Schärtl and H. Sillescu, J. Stat. Phys. **77**, 1007 (1994).
[56] T. M. Truskett, S. Torquato, S. Shastry, P. G. Debenedetti, and F. H. Stillinger, Phys. Rev. E **58**, 3083 (1998).
[57] G. S. Cargill III, Solid State Phys. **30**, 227 (1975).
[58] E. B. Sirota, H. Ou-Yang, S. K. Sinha, P. Chaikin, J. Axe, and Y. Fujii, Phys. Rev. Lett. **62**, 1524 (1989).
[59] S. Sachdev and D. R. Nelson, Phys. Rev. B **32**, 1480 (1985).
[60] W. Hess and R. Klein, Adv. Phys. **32**, 173 (1983).
[61] B. Chu, *Laser Light Scattering* (Academic Press, Orlando, FL, 1974).